remote sensing

MDPI

Article

Phase Spectrum Smoothing Demodulation: A New Frontier in eLoran Signal Processing for Enhanced Performance

Shiyao Liu [1,2,*], Baorong Yan [1,2], Yu Hua [1,2], Wudian Kou [1,2], Shougang Zhang [1,3,4], Lu Xu [5] and Jun Lu [5]

[1] National Time Service Center, Chinese Academy of Sciences, Xi'an 710600, China
[2] Key Laboratory of Precise Positioning and Timing Technology, Chinese Academy of Sciences, Xi'an 710600, China
[3] University of Chinese Academy of Sciences, Beijing 100039, China
[4] Key Laboratory of Time and Frequency Standards, Chinese Academy of Sciences, Xi'an 710600, China
[5] School of Software Engineering, Chengdu University of Information Technology, Chengdu 610225, China
* Correspondence: liushiyao@ntsc.ac.cn; Tel.: +86-13809182818

Abstract: In the field of modern navigation and positioning, the ground-based eLoran system, serves as a vital backup to the global navigation satellite system (GNSS), which is crucial for numerous key applications. Signal demodulation, integral to eLoran's precision timing and information transmission, significantly affects system performance. Aiming at the pulse position modulation (PPM) characteristics of eLoran signals, this paper introduces an innovative phase spectrum smoothing demodulation (PSSD) algorithm, crafted to improve demodulation performance under complex noisy and interference-laden conditions. Following a systematic review of existing demodulation techniques in eLoran, this paper details the theoretical foundation, key steps, and significant impact of parameter selection for the PSSD algorithm. Then, the unique advantages in dealing with noise, continuous wave, and skywave interference are analyzed and verified. Through extensive experimental validation under various SNR and interference conditions, the PSSD algorithm shows significant superiority in demodulation performance compared with the traditional envelope phase detection (EPD) algorithm. The effectiveness of the PSSD algorithm in interference mitigation and its stable performance across diverse conditions confirm its potential to meet the high-precision timing requirements of eLoran systems, contributing to the advancement of modern communication systems.

Keywords: eLoran; phase spectrum smoothing demodulation; signal reception processing; modern communication systems

Citation: Liu, S.; Yan, B.; Hua, Y.; Kou, W.; Zhang, S.; Xu, L.; Lu, J. Phase Spectrum Smoothing Demodulation: A New Frontier in eLoran Signal Processing for Enhanced Performance. *Remote Sens.* **2024**, *16*, 4700. https://doi.org/10.3390/rs16244700

Academic Editors: Mattia Crespi, Benedikt Soja and Maria Kaselimi

Received: 1 November 2024
Revised: 11 December 2024
Accepted: 15 December 2024
Published: 17 December 2024

1. Introduction

In the present era, the global navigation satellite system (GNSS) acts like an invisible net, providing us with high-precision positioning, navigation, and timing (PNT) services. Its significance is evident [1,2]. However, much like a double-edged sword, while GNSS brings convenience, its vulnerability to various interferences and spoofing attacks poses a threat to applications in related fields [3–6]. This vulnerability compels us to reevaluate the reliability of PNT services and information transmission, prompting us to actively explore reliable alternative or complementary technologies. In this context, the enhanced Loran (eLoran) ground backup system emerges. The eLoran system, with its strong anti-interference ability, wide coverage, stability, and excellent performance, serves as an important supplement and backup for the GNSS system [7–10]. In recent years, many countries around the world have actively engaged in or resumed development of the eLoran system. This trend indicates that the establishment and advancement of the eLoran system are not only inevitable requirements for the construction of time–frequency systems in various countries but also indispensable and crucial parts of enhancing the national satellite–ground integrated PNT system [11–13].

In eLoran receivers, demodulation is a crucial signal processing module, directly affecting the accuracy of timing and information transmission. Globally, scholars have extensively researched eLoran demodulation technology. Currently, the commonly used eLoran demodulation technology is the envelope phase detection (EPD) method [14]. It extracts phase differences by sampling the envelopes of two orthogonal signal paths to achieve demodulation, but has limitations in anti-interference and noise resistance. In 2007, Lo et al. proposed the signal matching correlation–pulse position detection (SMC-PPD) algorithm based on signal sliding correlation in the time domain [15]. However, as noise and interference increase, the error frequency of peak position detection significantly rises, leading to a higher bit error rate. In 2020, Yuan et al. proposed the envelope correlation–phase detection (EC-PD) algorithm, which combines two envelope correlation schemes for different scenarios [16]. It studies the impact of skywave on signal-to-noise ratio (SNR) gain and switches adaptively based on it, improving modulation performance to some extent. However, it remains in the time domain phase demodulation category. In 2022, Lyu et al. proposed an algorithm based on the log likelihood ratio (LLR) [17]. It calculates and compares the probability of each bit, skips the demodulation process, and improves the decoding success rate to a certain extent. However, it does not consider the impact of various interference environments on probability calculations and requires further derivation and verification. In 2024, our research achieved a remarkable breakthrough by successfully introducing machine learning into eLoran demodulation research. We deeply explored and proposed the application of machine learning algorithms like MSVM. The experimental results show their excellent performance and application potential. However, due to resource limitations, they could not be fully implemented, tested, and optimized, and thus were not used as comparison objects in this paper [18].

To enhance the performance of eLoran receivers in complex electromagnetic environments such as continuous wave interference (CWI) and high noise levels, and to ensure the functional realization of eLoran system, this study introduces an innovative phase spectrum smoothing demodulation (PSSD) algorithm from a new perspective. Based on the pulse form and spectral characteristics of eLoran signal, the PSSD algorithm employs advanced time–frequency domain signal processing techniques to minimize the impact of noise and interference. By leveraging phase difference discrimination in the frequency domain, it aims to enhance the accuracy and reliability of signal demodulation.

The similar spectral smoothing technology finds extensive applications in other signal processing fields, such as audio signal processing (noise reduction, echo cancellation, and audio enhancement), image processing (image restoration, denoising, and super-resolution imaging), communication systems (improving signal transmission reliability and efficiency by resisting multipath interference and frequency-selective fading), as well as biomedical imaging, radar signal processing, seismic data processing, and astronomy data analysis [19–26]. The introduction of PSSD is also of far-reaching significance, making a substantial contribution to promoting the development and application of the eLoran system and related fields, mainly involving the following three aspects.

Firstly, in terms of technological innovation, the PSSD algorithm brings new ideas and methods for eLoran demodulation technology. It integrates advanced signal processing concepts and introduces a combined time–frequency domain processing approach, expanding the boundaries of signal processing and leading the technological development direction in this field.

Secondly, in terms of system performance improvement, it significantly enhances the stability of the eLoran system in harsh environments, improves timing accuracy and information transmission capabilities, endows the system with stronger environmental adaptability, and meets users' demands for high-precision PNT services.

Thirdly, in terms of promoting industry development, it helps to promote the upgrading of eLoran-related industries, provides new technical support for industrial development, drives the development of related fields such as communication and navigation,

promotes technological integration among various fields, and cultivates professional talents, providing guarantees for the sustainable development of the industry.

In the following sections, we will elaborate on the principles and implementation of the PSSD algorithm, as well as present the experimental results and performance analysis.

2. Background Principles

2.1. ELoran Signal System

The eLoran system is an internationally standardized ground-based radio system [27,28], an advanced iteration of the Loran-C system incorporating Eurofix data-link techniques [29]. Operating within the frequency band of 90 to 110 kHz with a central carrier frequency of 100 kHz, the eLoran system ensures stable and reliable signal transmission. The most significant improvement in the system was achieved by modulating information onto the third to eighth pulses of each pulse group, thereby achieving efficient data communication. The standard current waveform at the base of the eLoran signal transmitting antenna is defined by Formula (1) [30].

$$s(t) = \begin{cases} A(t-\tau)^2 \exp\left(-2\frac{(t-\tau)}{65}\right)\sin(2\pi f_c t + P_c), & \tau \ll t \ll 65+\tau \\ 0, & t < \tau \end{cases} \quad (1)$$

where A is a constant related to the peak amplitude; t is the time in μs; τ is the envelope-to-cycle difference in μs; f_c = 100 kHz is the carrier frequency, and P_c = 0 or π is the phase code parameter, in radians. According to the above definition, Figure 1 shows the standard Loran C pulse waveform and the normalized amplitude spectrum.

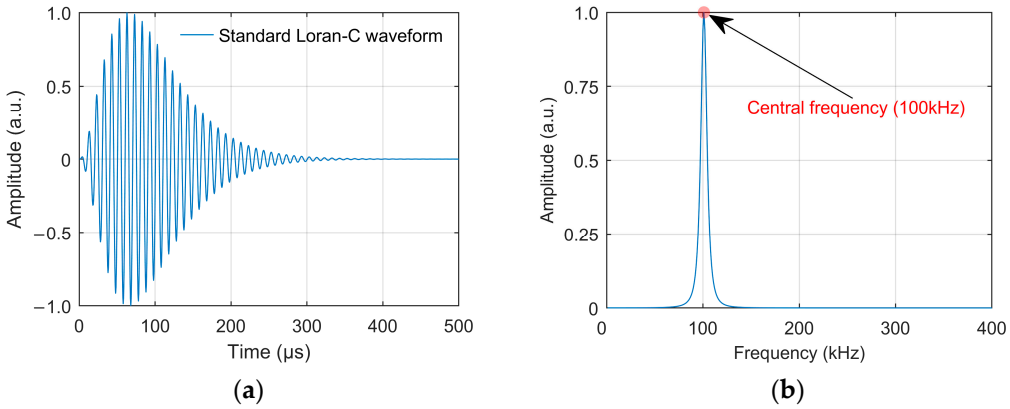

Figure 1. Standard Loran-C signal: (**a**) normalized signal waveform; (**b**) normalized amplitude spectrum.

The signal-to-noise ratio (SNR) of the Loran-C signal has its specific definition. It refers to the ratio of the signal received level to the root mean square level value of the atmospheric noise, and can be expressed as a dimensionless number or in decibels. Among these, the signal level is defined as the effective value level of the continuous wave at 25 μs after the starting point of the pulse envelope [31]. The SNR in the subsequent simulations of this paper is all based on the above definition as the standard.

Each station chain in the eLoran system consists of a master station and several sub-stations, distinguished by a unique group repetition interval (GRI) that facilitates rapid identification and precise timing [32,33]. Both the master station and the sub-station have two pulse group phase coding formats of A and B law (A_{master}, B_{master} and A_{sub}, B_{sub}), alternated in a cyclical pattern for broadcasting, respectively [34,35].

By leveraging Eurofix data-link technology, the eLoran system introduces three-state pulse position modulation (PPM) with time modulation quantities of 0 or ±1 μs, as shown in Figure 2 [36,37]. This modulation takes advantage of the eLoran signal's pulse characteristics to form frame information.

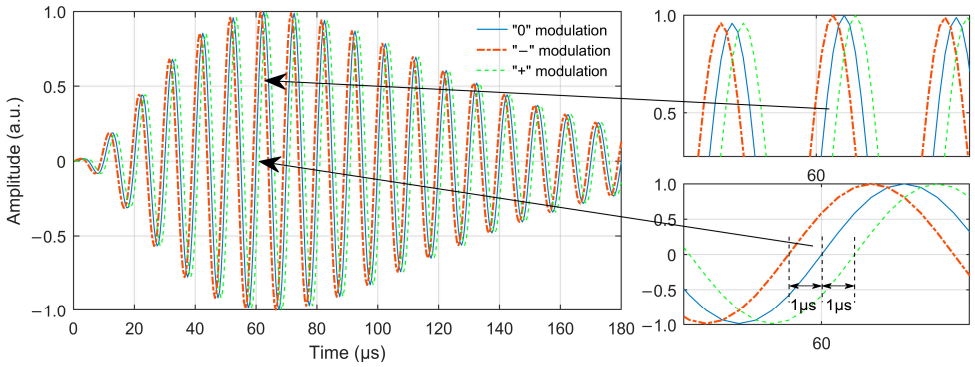

Figure 2. Three-state PPM diagram of eLoran signal.

The frame construction is meticulously designed to carry information through a specific modulation method based on the 128-character ASCII code [38]. Each frame consists of 30 pulse groups with 180 modulated pulses. In each pulse group, the modulation status of six pulses (third to eighth) corresponds to an ASCII character pattern and is converted into a 7-bit binary code, enabling each frame to convey 210 bits of information [27]. It also lays the groundwork for the dissemination of time code information and the potential sharing of additional data, such as differential correction values, in the future.

The construction of frame information is designed to be resilient against common transmission errors and interference. By integrating Reed–Solomon (RS) codes and Cyclical Redundancy Check (CRC) codes with powerful error correction capabilities, the system's robustness is remarkably enhanced, providing a firm foundation for the demodulation process [39–42].

2.2. Traditional EPD Algorithm

In the eLoran system, data acquisition hinges on demodulating the transmitted modulation elements to reconstruct the frame information. For eLoran signals with a carrier cycle of 10 μs, phase shifts of 0° or ±36° are generated by emissions of 1 μs that are on-time, early, or late. The EPD algorithm functions by assessing the phase differences at the time-domain sampling points between the modulated signal and the reference signal (the first pulse of group). It then converts these into corresponding modulation code words, and proceeds with decoding to obtain the final time code information. This is a fundamental logic used in eLoran receivers.

First of all, after the modulated signal passes through pre-processing modules (such as BPF and anti-interference) and the phase tracking module, the signal is divided into I and Q channels. Then, the I and Q branches interact with local sine and cosine carriers and undergo low-pass filtering, thereby preserving the sine and cosine components of the modulation phase and phase offset. The resulting quadrature sampled data are denoted as (a_i, b_i), with the reference signal's phase offset captured as (a_i^{ref}, b_i^{ref}). Using these data, the phase difference (α-β) is calculated through Formulas (2)~(4).

$$\begin{cases} tan\alpha_i = sin\alpha_i / cos\alpha_i = a_i / b_i \\ tan\beta_i = sin\beta_i / cos\beta_i = a_i^{ref} / b_i^{ref} \end{cases} \tag{2}$$

$$tan(\alpha_i - \beta_i) = \frac{tan\alpha_i - tan\beta_i}{1 + tan\alpha_i tan\beta_i} = \frac{a_i b_i^{ref} - b_i a_i^{ref}}{a_i a_i^{ref} + b_i b_i^{ref}} \tag{3}$$

$$\alpha_i - \beta_i = arctan\left(\frac{a_i b_i^{ref} - b_i a_i^{ref}}{a_i a_i^{ref} + b_i b_i^{ref}}\right) \tag{4}$$

where α_i and β_i represent the phase of the modulated signal and the reference signal at the i-th sampling point, respectively, and $\alpha_i - \beta_i$ is the corresponding phase difference.

Following this, the algorithm uses multi-threshold processing, set at ±18°, to ascertain the polarity of the phase difference. Phase differences within the −18°~18° range are deemed "0" modulation; those surpassing 18° are labeled as "+" modulation; and those falling below −18° are recognized as "−" modulation. Ultimately, based on the statistical outcomes from N sampling points, the modulation state is determined by a majority decision, with error correction applied according to the principle of balanced modulation when an equal number of modulation states occur [18,43].

Despite its wide usage, the EPD algorithm faces inherent limitations. As a time-domain method, it requires high signal quality. However, eLoran signals are prone to electromagnetic interference such as noise and CWIs, which causes severe waveform distortion and phase detection errors, consequently affecting the decoding success rate. Also, as an AM signal, the eLoran signal is not sampled on a perfect 100 kHz carrier, introducing a certain bias in the 36° phase detection itself.

The example provided in Figures 3 and 4 illustrates the impact of noise and CWI on signal waveform and the resulting phase difference curve after EPD demodulation. In this pulse group, the correct modulation is "− 0 + 0 0 0". However, due to the phase difference often being within the wrong threshold range, the fourth, sixth, and seventh pulses are all wrongly demodulated as "+" modulation. As the power of CWI and noise increases, these fluctuations become more pronounced. This highlights the limitations of the EPD algorithm and the potential errors in practical applications.

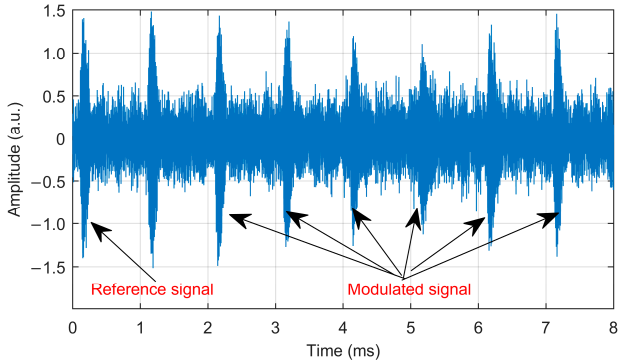

Figure 3. Influence of noise and CWIs on time-domain waveform of eLoran pulse group.

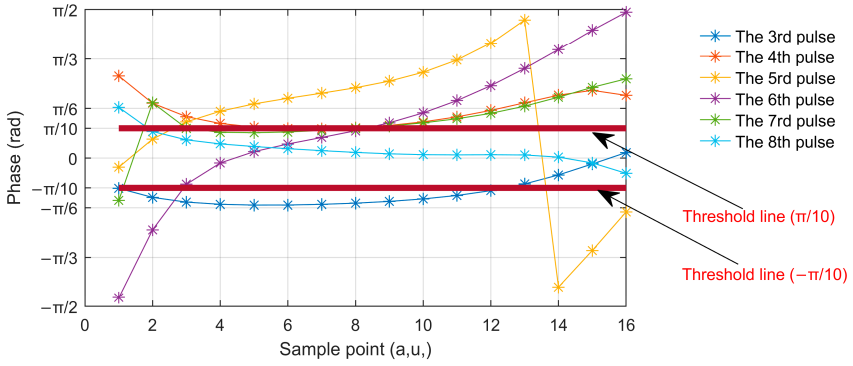

Figure 4. Phase difference curves of each pulse under EPD algorithm (SNR = 10 dB, 2 CWIs).

Having evaluated the limitations of the EPD algorithm in the eLoran system, it is clear that advanced demodulation techniques are urgently needed. These techniques should address noise and interference issues while enhancing the reliability and precision of the system. In the next section, we will explore innovative methods to overcome these challenges and improve demodulation performance.

3. Method Description

Building on the insights from the previous section, this section introduces a suite of advanced demodulation algorithm designed to bolster the signal processing capabilities of the eLoran system. Starting with a detailed explanation of the principles and steps of the algorithm, the advantages of the method in anti-interference and its effectiveness in real scenes is further studied.

3.1. Phase Spectrum Smoothing Demodulation

Phase detection demodulation technology is widely used in eLoran receivers. As introduced in Section 2.2, the EPD algorithm relies on time-domain phase detection and typically employs a BPF to improve signal quality. However, it has great limitations when dealing with in-band noise and CWIs. To overcome these challenges, this paper proposes a novel phase spectrum smoothing demodulation (PSSD) algorithm based on phase spectrum filtering. This algorithm aims to more effectively suppress noise and interference through frequency domain processing, thereby enhancing the demodulation performance of eLoran signals. The following sections will detail its principles and steps.

1. Fast Fourier Transform (FFT) processing. For a given eLoran pulse signal $x(t)$, the FFT is performed to obtain its frequency domain representation $X(f)$, which includes the signal's amplitude and phase spectra. This information will be used for the next step of phase spectrum smoothing. The FFT operation can be mathematically represented as:
$$X(f) = FFT(x(t)) = \int_{-\infty}^{+\infty} x(t)e^{-j2\pi ft} \tag{5}$$
Notably, in the FFT process for eLoran signals, the choice and application of the truncation window are crucial. It is designed to pick out the effective portion of the signal and reduces the noise energy. This enables a more accurate frequency components analysis and lays the groundwork for subsequent phase smoothing processing.
2. Phase spectrum filtering. For the eLoran signal's specific bandwidth, the key frequency range components (denoted as L_{freq} in the frequency domain $X(f)$) are subjected to filtering. This process aims to maintain the integrity of the signal while enhancing its phase stability and mitigating the impact of noise and interference on the phase spectrum.
Let $H(f)$ represent the transfer function of the smoothing filter. The phase spectrum filtering can be mathematically expressed as:
$$X_{filt}(f) = X(f) \cdot H(f) \tag{6}$$
where $X_{filt}(f)$ represents the frequency domain signal after smoothing. The choice of the smoothing filter's length and shape is critical, as it dictates the degree of smoothing applied. The appropriate Gaussian window filter is selected through experimentation, which effectively smooths the phase spectrum, reducing noise levels and controlling phase jumps. This is crucial for the subsequent calculation of phase differences, ensuring that the signal information used is both stable and reliable.
3. Phase difference vector acquisition. The purpose of this step is to calculate the phase difference between the test signal and the reference signal within the frequency domain. By comparing the complex spectra within the range of L_{freq}, a phase difference vector that reflects the changes in phase shift between the two signals can be obtained. Moreover, it is necessary to address the discontinuity of the phase vector caused by 2π jumps.
For $X_{filt,test}(f)$ and $X_{filt,ref}(f)$ in the frequency domain, calculate the phase vector according to the real and imaginary parts of each frequency point as follows:
$$\varphi_{test}(f) = phase\Big(X_{filt,test}(f)\Big) \tag{7}$$

$$\varphi_{ref}(f) = phase\Big(X_{filt,ref}(f)\Big) \tag{8}$$

Given the phase $\varphi(f)$ at frequency point f, the unwrapping process is mathematically defined to correct for discontinuities due to 2π jumps. Specifically, for each frequency point f, the phase is adjusted as follows:

- If $\varphi(f) - \varphi(f-1) > \pi$ in the positive direction:

$$\varphi(f) \leftarrow \varphi(f) - 2\pi \tag{9}$$

- Alternatively if $\varphi(f) - \varphi(f-1) < -\pi$ in the negative direction:

$$\varphi(f) \leftarrow \varphi(f) + 2\pi \tag{10}$$

The unwrapping operation is applied to both $\varphi_{test}(f)$ and $\varphi_{ref}(f)$, yielding the unwrapped phases $\varphi_{test,unwrapped}(f)$ and $\varphi_{ref,unwrapped}(f)$, respectively. This process involves adjusting the phase at each frequency point to ensure continuity. Subsequently, the phase difference vector $\Delta\varphi(f)$ is calculated as:

$$\Delta\varphi(f) = \varphi_{test,unwrapped}(f) - \varphi_{ref,unwrapped}(f) \tag{11}$$

This approach ensures a continuous and consistently oriented representation of the phase difference, which is essential for reliable frequency domain analysis.

4. Weighted phase difference calculation. Considering the PPM characteristics of eLoran AM signals, the phase difference curves obtained from different modulated signals exhibit a predominantly linear trend with different slopes in the frequency band, and are symmetrically distributed near the 100 kHz frequency point.
   Based on this feature, a suitable normalized weighting window is selected. Through testing multiple window functions, the Gaussian window is chosen for its optimal performance and is configured with suitable parameters to perform a weighted summation on the phase difference vector $\Delta\varphi(f)$, resulting in a single weighted phase difference.

$$\Delta\Phi_{weighted} = \sum_f \Delta\varphi(f) \mathrm{e}^{-\frac{1}{2}\left(\frac{f-f_c}{\sigma}\right)^2} \tag{12}$$

   Subsequently, the weighted phase difference $\Delta\Phi_{weighted}$ is unwrapped in the range $-\pi/2$ to $\pi/2$ to obtain $\Delta\Phi$, ensuring an effective demodulation range.

5. Modulation decision. Utilize the obtained $\Delta\Phi$ to determine the modulation state of the eLoran signal through the modulation decision process. The modulation decision criteria are consistent with the EPD algorithm. Based on the value of $\Delta\Phi$, apply the following decision criteria:
   - If $\Delta\Phi \geq \pi/10$, then the modulation decision is "+".
   - If $-\pi/10 < \Delta\Phi < \pi/10$, then the modulation decision is "0".
   - If $\Delta\Phi \leq -\pi/10$, then the modulation decision is "−".

A flowchart based on the above algorithm steps is shown in Figure 5. It is evident that the FFT signal length, FFT resolution, signal bandwidth selection, and Gaussian window σ are key parameters affecting the algorithm's performance in this study. They collectively determine the accuracy, stability, and computational efficiency of signal processing. We have selected the following parameter values as relatively optimal configurations based on an in-depth understanding of eLoran signal characteristics, previous design research experience with eLoran receivers, and meticulous experimental analysis of parameter sensitivity.

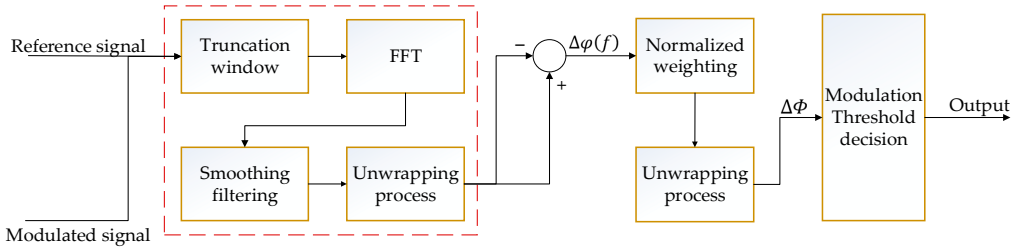

Figure 5. Flowchart of PSSD algorithm.

1. **FFT Signal Length**: The width of the truncation window U is set at 170 μs (specifically, from −42.5~127.5 μs centered on the highest point of the standard signal). This selection considers the pulse characteristics, effective duration, and SNR of the eLoran signal.
2. **FFT Resolution**: Extensive experiments showed that increasing the FFT resolution (e.g., by 100 Hz) does not significantly improve demodulation performance. Therefore, a resolution of 1 kHz is set for the FFT, which balances the frequency resolution with a sampling rate of f_s = 2 MHz and computational efficiency.
3. **Signal Frequency Bandwidth**: The phase spectrum processing is focused on the L_{freq} = 92~108 kHz band, which covers the main frequencies and high-power components of the eLoran signal.
4. **Gaussian Window**: Based on experiments, considering the spectral characteristics and central frequency selectivity of the signal, we have adopted two sets of different Gaussian window parameters:
    - Phase Spectrum Smoothing: The window width is set to 5 (corresponding to 5 kHz), and σ is set to 1.5. This parameter selection aims to effectively smooth the signal's phase spectrum while maintaining its spectral characteristics.
    - Phase Difference Weighted Summation: The window width is set to 17 (corresponding to 17 kHz), and σ is set to 2. This parameter selection helps to improve the accuracy of the weighted phase difference in summation process.

Experimental results indicate that the selected parameters demonstrate high performance and good robustness of the algorithm under a variety of signal environments and interference conditions, proving the rationality of our parameter selection.

The PSSD algorithm offers a more effective approach to demodulation in eLoran systems by addressing the limitations of traditional methods. Its frequency domain processing and carefully selected parameters enhance the signal's stability and accuracy, providing a promising solution for improved demodulation performance.

3.2. SNR Gain

In eLoran systems and other radio systems, noise significantly impacts signal demodulation performance. SNR gain, which enhances the signal strength relative to noise during demodulation through specific algorithms or techniques, is crucial for improving the system's demodulation accuracy and reliability.

The EPD algorithm, although improving the SNR to some extent through BPF, is evidently insufficient in handling in-band noise. Particularly in high-intensity noise environments, the residual noise energy can cause signal distortion and adversely affect demodulation accuracy. In sharp contrast, the newly proposed PSSD algorithm showcases significant advantages in handling in-band noise, especially under low SNR conditions.

The PSSD method leverages phase difference information from the in-band phase spectrum for demodulation. Firstly, a truncation acquisition technology is employed to collect the useful segment of the signal by means of windowing and perform FFT, effectively reducing noise and interference energy. Subsequently, a Gaussian window is used to smooth the effective part of the spectrum, further enhancing the in-band SNR. This

processing method cleverly combines the unique pulse characteristics of eLoran signal waveform and the shape characteristics of the broadband amplitude spectrum.

In order to quantify the improvement in demodulation performance brought by this gain, we introduce a new metric, "Effective Signal-to-Noise Ratio" (ESNR), defined as the ratio of eLoran signal power P_{signal_inband} to noise power P_{noise_inband} within the effective bandwidth L_{freq} (92~108 kHz), as shown in Equation (1). This metric is specifically designed to assess the performance of eLoran signals in the key frequency range and can provide an intuitive reflection of the power dynamics within the effective bandwidth.

$$\mathrm{ESNR} = \frac{P_{signal\_inband}}{P_{noise\_inband}} \tag{13}$$

To illustrate the advantages of the truncation window and spectral smoothing in PSSD algorithm, an example under SNR = −10 dB white noise environment is presented.

Figure 6 depict the phase difference vector curves for three different modulations. It is evident that these curves, post-truncation window sampling and spectral smoothing filtering, exhibit remarkable smoothness, closely resembling noise-free conditions, effectively reducing the risk of phase jumps. In contrast, without truncation and smoothing, the phase fluctuates dramatically. In Figure 6b,c, the weighted phase differences are calculated as 0.0485π and 0.2871π, respectively, which are within the wrong threshold range, leading to incorrect modulation decisions of "0" and "+".

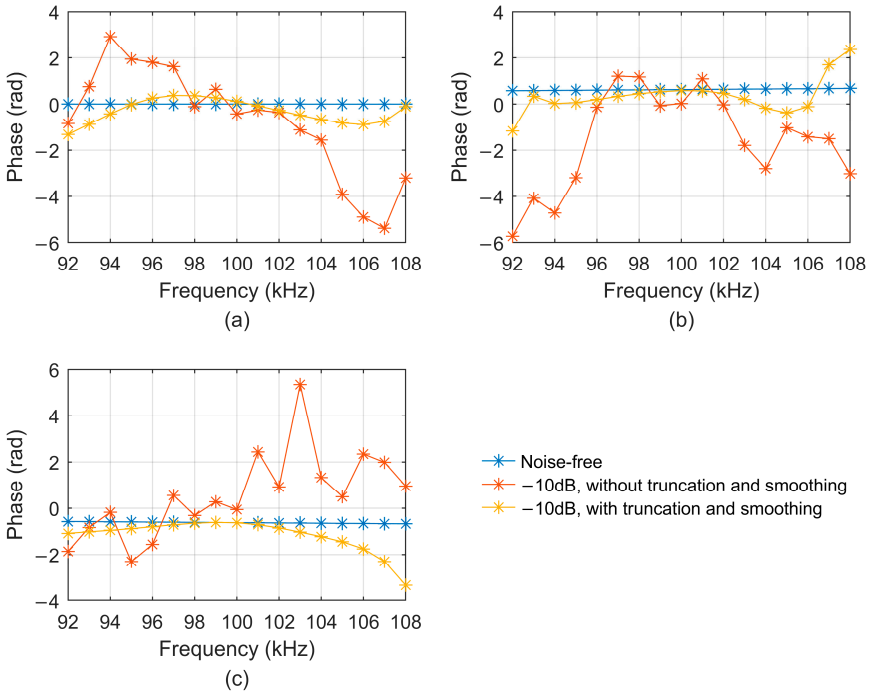

Figure 6. Phase difference vector of: (**a**) "0" modulation; (**b**) "+" modulation; (**c**) "−" modulation.

Furthermore, we modulated the eLoran pulse group with time codes and added white noise with different SNRs. Conducting multiple sets of experiments according to the algorithm steps. Meanwhile, using Formula (13), we can accurately estimate the ESNR in frequency domain before and after filtering, thereby deriving the statistical mean value of ESNR gain, ΔESNR, and combining it with demodulation accuracy rate (DAR) for in-depth discussion. The above types of data are comprehensive organized in Table 1.

Table 1. ESNR gain and DAR performance improvement statistics of PSSD algorithm.

SNR	ESNR (dB)		ΔESNR (dB)	DAR (%)		
	Before Filtering	After Filtering		PSSD with WS	PSSD Without WS	EPD
−20	−10.18	−1.17	9.01	43.04	32.55	33.47
−15	−5.12	3.86	8.98	63.05	33.81	45.32
−10	−0.11	9.03	9.14	84.61	52.94	68.40
−5	4.82	13.92	9.10	98.17	92.89	91.46
0	9.92	18.97	9.05	100	99.98	99.65
5	14.87	23.94	9.07	100	100	100
10	19.87	28.86	9.00	100	100	100

WS = truncation window sampling and spectral smoothing filtering.

As indicated by Table 1, under different SNRs, there is a significant gain in ESNR, which is further converted into an improvement in demodulation performance. For instance, at SNR = −10 dB, ΔESNR is 9.14 dB. Compared with the case without truncation window and smoothing, the DAR of PSSD algorithm remarkably increases from 52.94% to 84.61%, while that of the EPD algorithm is only 68.40%. In addition, in other SNR environments, a similar conclusion can be drawn, and the lower the SNR, the more significant the improvement in demodulation performance.

The comparative analysis in this section covers noise environments within different SNR ranges and aims to demonstrate the new algorithm's theoretical correctness. Experimental results firmly establish the new algorithm's effectiveness in handling in-band noise and its superiority in demodulation accuracy, especially its application potential under low SNR conditions.

3.3. CWI Resistance

In the practical application of eLoran systems, CWI is a common and challenging issue, often originating from other radio equipment or intentional jamming activities. CWI potentially poses a direct threat to signal quality and demodulation accuracy.

As previously discussed, the EPD algorithm relies on BPF that are ineffective against in-band noise and CWI. Although digital signal processing techniques can provide some suppression of in-band interference, a considerable amount of residual often persists. Additionally, the use of analog notch filtering, while aimed at mitigating interference, can also inadvertently damage the spectral integrity, resulting in signal distortion. In contrast, the PSSD algorithm utilizes advanced interference suppression techniques. As detailed in Section 3.1, it employs truncation windows to reduce interference energy and employs spectral smoothing filtering to further decrease the interference modulus power, significantly enhancing the system's resistance to CWI.

To demonstrate the interference suppression advantages of the PSSD algorithm, two sets of experimental examples are provided (see Section 4.1 for CWI parameter settings):

a. Noise-free scenario, "−" modulation, 2 CWIs are introduced to compare the impact of different processing methods on phase difference stability.
   Figure 7 illustrates that without truncation windows and phase smoothing, the method cannot effectively resist CWI even in a noise-free environment, leading to unstable phase differences and potential demodulation errors. In contrast, after the truncated window and smoothing with Gaussian weight coefficient, the amplitude spectrum and phase difference curve (yellow lines) are smoother, restraining interference and maintaining demodulation accuracy to some extent. Calculation reveals that the weighted phase differences from the red and yellow phase difference curves are -0.0973π and -0.1411π respectively. Accordingly, based on the threshold ($-\pi/10$), incorrect ("0") and correct ("−") demodulation results are obtained, respectively.

b. SNR = −10 dB white noise scenario with 2 CWIs (matching the settings from example a); the DARs are compared to evaluate the different processing methods.
Figure 8 showcases the statistical results of multi-groups of experiments. When SNR = −10 dB and CWI exist, the average DAR of PSSD algorithm stands at 74.91%, which is notably higher than 61.99% of the EPD algorithm. This further validates the new algorithm's ability to resist CWIs in a low SNR environment. The results depicted in Figure 8 provide solid evidence of the effectiveness and robustness of the PSSD algorithm in handling challenging interference conditions.

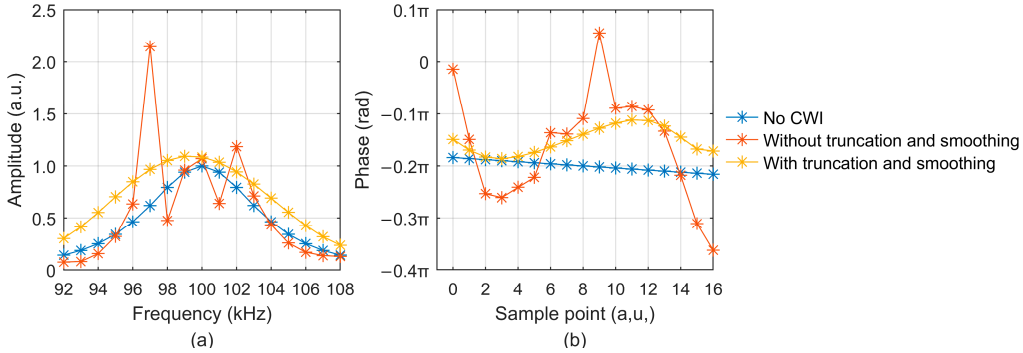

Figure 7. Feature comparison under different processing methods: (**a**) amplitude spectrum; (**b**) phase difference curve.

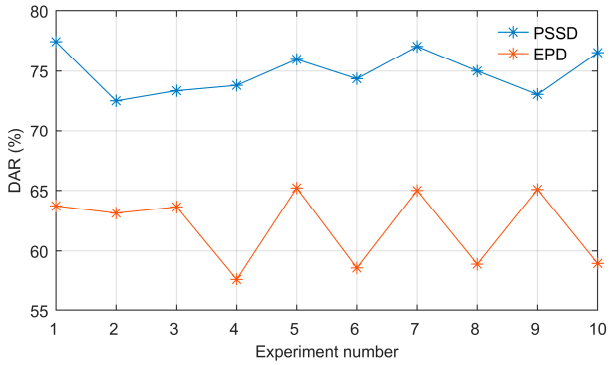

Figure 8. DAR results of multi-group experiments.

This section is underpinned by experimental examples, which affirm the effectiveness of the PSSD algorithm in countering CWI. In both noise-free and low SNR scenarios, the algorithm's phase smoothing processing proficiently sustains phase difference stability and notably augments demodulation capabilities. When compared with the EPD algorithm, the PSSD algorithm exhibits outstanding superiority in anti-CWIs. In Section 4, more comprehensive performance analysis under diverse interference conditions will be presented to further illustrate the robustness of the PSSD algorithm.

3.4. Skywave Interference Resistance

This section assesses the impact of skywave interference on the PSSD algorithm and demonstrates its effectiveness in countering such interference.

Skywave interference, a prevalent form encountered in eLoran system operation due to signals reflected from the ionosphere with highly uncertain intensities, can pose challenges. When intense skywave interference is close to ground wave signals, the mixed signal can be difficult for eLoran receivers to separate, potentially leaving residual interference that accurate realization of the subsequent signal processing module functions.

Theoretically, beyond environmental noise, given that the test and reference signals are subjected to skywave interference of identical intensity and position, the waveform

distortion remains consistent. Therefore, it can be deemed that skywave exerts negligible influence on the demodulation process, a concept that has been confirmed within EPD algorithms. The PSSD algorithm analyzes signals in the frequency domain via FFT processing. Assuming the test and reference signal are subjected to the same degree of skywave interference, it can be expected that the characteristics of phase difference $\Delta\Phi$ of the mixed signals $x_{ref,mix}(t)$, $x_{text,mix}$ should be similar to those without skywave, thus theoretically eliminating the influence of skywave interference on demodulation.

To substantiate the theoretical rationale outlined previously and the effectiveness of PSSD algorithm in handling skywave interference, we analyzed the impact of different intensities of skywave on the phase difference. First, in a noise-free environment, we studied its effects on the PSSD theory through experiments. Specifically, delay difference: 40~160 μs, step size: 0.5 μs; and sky-to-groundwave ratio (SGR): 6 dB and 12 dB.

Figure 9 depicts the variations in $\Delta\Phi$ under different skywave interferences. In the two subfigures, the mean values of $\Delta\Phi$ for "+", "0", and "−" modulations are 0.1998π, 0, -0.2005π and 0.1999π, 0, -0.2003π respectively. The deviations from the no-skywave scenario (0.1997π, 0, -0.2007π) do not exceed $\pi/250$. The results indicate that, even under skywave interference, after phase spectrum smoothing, the PSSD algorithm can still accurately capture the original characteristics of the signal. Regardless of its position and SGR, the impact of strong skywave interference on the trend of $\Delta\Phi$ is negligible, thus ensuring the correctness of demodulation. In addition, more experiments found that skywave brings a power gain effect to the mixed signal, changing the SNR. When skywave and groundwave are in phase, the SNR and demodulation accuracy increase. Conversely, when out of phase, they decrease. This phenomenon occurs in both the PSSD and EPD algorithms. However, as shown in Figure 9, skywave interference does not impact the phase difference or the algorithm itself. In reality, there are also skywave separation techniques to minimize its impact on eLoran systems [13].

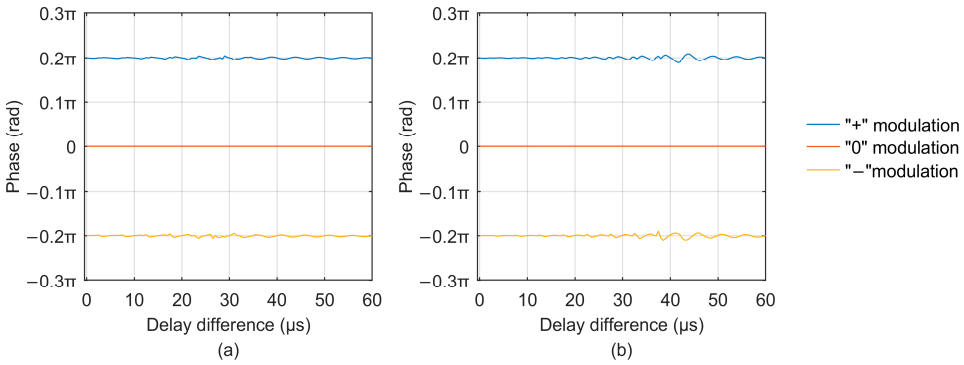

Figure 9. Diagram of weighted phase difference: (**a**) SGR = 6 dB; (**b**) SGR = 12 dB.

Drawing from the above theoretical discussions and empirical results, it can be concluded that the PSSD algorithm can effectively resist skywave interference and safeguard the accuracy of the demodulation process. This discovery indicates that in subsequent simulation experiments, skywave interference is no longer a critical factor requiring special attention. Thus, we can focus on optimizing the algorithm's performance and evaluating its performance in different practical scenarios. Combined with the PSSD algorithm's ability to deal with in-band noise and CWIs, this makes it an all-encompassing and potent demodulation method for eLoran systems.

4. Experimental Results and Performance Analysis

4.1. Experiment Design

Building upon the analysis of the theory of PSSD algorithm and its anti-interference capabilities in previous sections, this section aims to comprehensively evaluate its demodu-

lation performance advantages in diverse environments through a series of well-designed experiments. The experimental design is outlined bellow:

1. Experimental environment:
   All experiments were conducted on a high-performance computer with Windows 10 operating system, an Intel Core i7 processor, and 32 GB of memory. MATLAB R2017b was used as the experimental platform to ensure accurate and reproducible algorithm simulations. The experimental dataset simulated eLoran signals under different SNR and CWI conditions. DAR was the main performance evaluation metric.
2. Parameter Settings:
   - Input signal: Continuous modulated pulse group signals.
   - Data modulation: Standard time-code frame data modulation was adopted.
   - Sampling rate: 2 MHz.
   - Bandpass filter: Set to 90~110 kHz, specifically designed for the EPD algorithm to filter out-of-band noise and interference.
   - SNR: −20~10 dB white noise environment, with a step size of 1 dB.
   - CWI: 0–4 single-frequency interferences (C1, C2, C3, C4) with specific frequencies and SIRs. C1: 97.2222 kHz, −7 dB; C2: 101.3333 kHz, −10 dB; C3: 103.6666 kHz, −9.21 dB; C4: 99.1111 kHz, −8.24 dB. Each interference was introduced with a random initial phase. Since most of the interference energy has been removed during preprocessing, a moderate interference power can be set. In all experiments involving CWIs throughout this paper, they are labeled and combined sequentially (e.g., "1 CWI" refers to C1, "3 CWIs" refers to the combination of C1, C2, and C3)
   - Experimental reproducibility: To ensure the reliability of statistical results and reduce random errors, each set of experimental conditions was repeated 10 times, with each run consisting of 50 frames (9000 pulses to be detected).

4.2. Comprehensive Performance Analysis

Based on the well-designed experiments, the results below visually present the DAR comparison of PSSD and EPD algorithms under various interference conditions.

The eLoran system adopts the CRC-RS cyclic check and error correction coding method, and a DAR of 90% becomes a key indicator for stable decoding of eLoran receivers. The black marks in Figure 10 present the SNRs under this indicator (−8.4 dB and −5.3 dB respectively). It is evident in an interference-free environment that the PSSD algorithm optimizes the SNR benchmark for successful decoding by 3.1 dB.

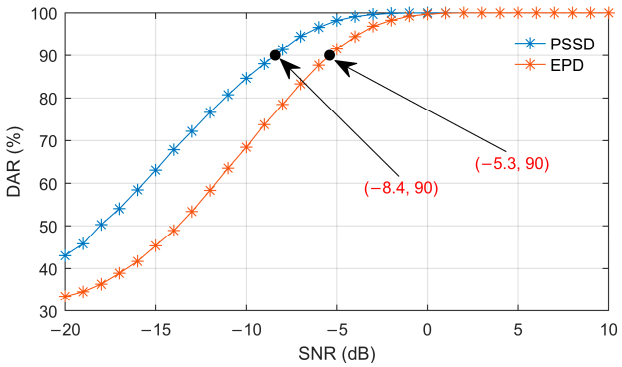

Figure 10. DAR comparison of PSSD and EPD algorithm without CWI.

Figure 11 presents the DAR comparisons of PSSD and EPD algorithm under different CWI conditions. Through this series of subfigures, we can systematically observe the change trends of DARs of the two algorithms as the number of CWIs increases. It highlights the significant anti-interference advantage of the new algorithm. Figures 10 and 11 cooperate with each other and jointly reveal the three primary trends:

1. Demodulation accuracy increases with higher SNR.
2. Fewer interferences correspond to higher demodulation accuracy rates.
3. The PSSD algorithm outperforms the EPD algorithm under all test conditions.

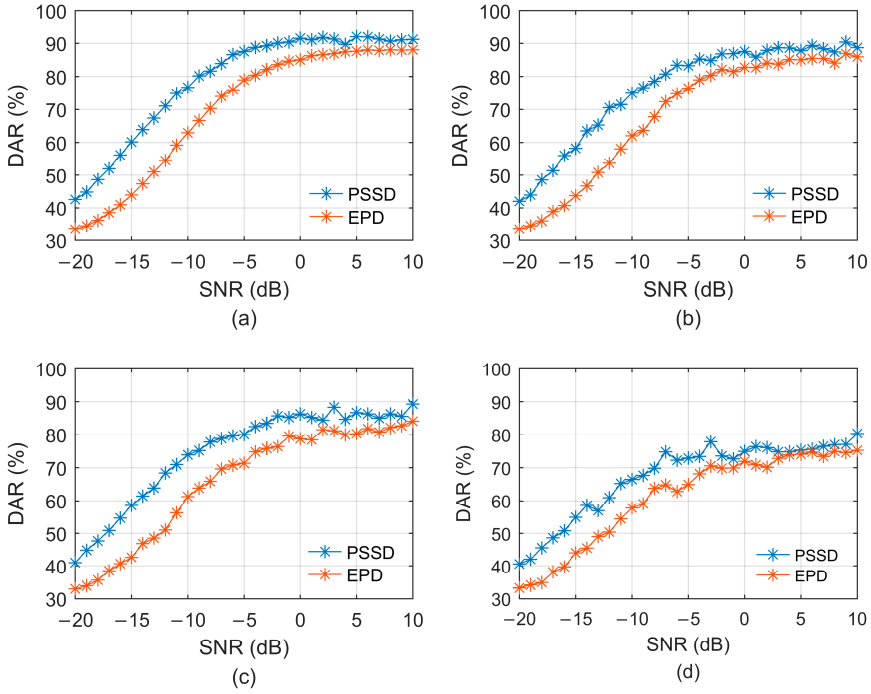

Figure 11. DAR comparison of PSSD and EPD with: (**a**) 1 CWI; (**b**) 2 CWIs, (**c**) 3 CWIs; (**d**) 4 CWIs.

Tables 2–6 provide detailed information on the performance improvements of the new PSSD algorithm over the EPD algorithm at different SNR intervals, further confirming the aforementioned trends and quantifying the performance enhancements within specific SNR ranges.

Table 2. Average DAR (%) statistics of PSSD and EPD algorithm without CWI.

SNR Range (dB)	DAR (%)		Gain (%)
	PSSD	EPD	
−20~−15	52.45	38.39	14.06
−15~−10	74.18	56.31	17.87
−10~−5	92.22	80.51	11.71
−5~0	99.44	96.63	2.81
0~5	100	99.92	0.08
5~10	100	100	0

Table 3. Average DAR (%) statistics of PSSD and EPD algorithm with 1 CWI.

SNR Range (dB)	DAR (%)		Gain (%)
	PSSD	EPD	
−20~−15	50.73	37.93	12.80
−15~−10	68.99	53.15	15.84
−10~−5	82.76	71.43	11.33
−5~0	89.59	82.46	7.13
0~5	91.21	86.64	4.57
5~10	91.34	87.92	3.42

Table 4. Average DAR (%) statistics of PSSD and EPD algorithm with 2 CWIs.

SNR Range (dB)	DAR (%)		Gain (%)
	PSSD	EPD	
−20~−15	50.04	37.88	12.16
−15~−10	67.33	52.51	14.82
−10~−5	79.59	69.48	10.11
−5~0	85.77	80.36	5.41
0~5	87.72	83.88	3.84
5~10	88.67	85.46	3.21

Table 5. Average DAR (%) statistics of PSSD and EPD algorithm with 3 CWIs.

SNR Range (dB)	DAR (%)		Gain (%)
	PSSD	EPD	
−20~−15	49.62	37.39	12.23
−15~−10	66.21	51.12	15.09
−10~−5	77.59	67.14	10.45
−5~0	83.88	76.13	7.75
0~5	85.94	80.04	5.90
5~10	86.53	81.97	4.56

Table 6. Average DAR (%) statistics of PSSD and EPD algorithm with 4 CWIs.

SNR Range (dB)	DAR (%)		Gain (%)
	PSSD	EPD	
−20~−15	47.10	37.39	9.71
−15~−10	60.52	50.19	10.33
−10~−5	70.67	62.19	8.48
−5~0	74.23	69.24	4.99
0~5	75.42	72.31	3.11
5~10	76.99	74.51	2.48

According to the statistics in the table, we can clearly see the advantages of PSSD algorithm, and draw the following conclusions:

1. Impact of SNR: The demodulation accuracy is positively correlated with SNR. Throughout the increase from −20 dB to 10 dB, the PSSD algorithm consistently shows superior performance.
2. Analysis of the impact of CWI numbers: As the number of CWI increases, the DAR values gradually decrease. For instance, within the SNR range of −10~−5 dB, the average DARs for different numbers of interferences are 82.76%, 79.59%, 77.59%, and 70.67%, respectively, showing a clear downward trend. This indicates that the presence of CWI negatively affects the demodulation process, with stronger interferences leading to greater negative impacts.
3. Advantage of PSSD algorithm in dealing with CWIs: The PSSD algorithm exhibits outstanding anti-interference capabilities when facing different levels of CWIs and can better maintain the demodulation performance. For instance, in the −10~−5 dB interval, as the number of CWI increases from 1 to 4, the DAR differences between the PSSD and EPD algorithms are 11.33%, 10.11%, 10.45%, and 8.48% respectively. This indicates that the unique technologies of PSSD, like truncated window sampling and spectral smoothing, play a crucial role in handling interference and make it outstanding in a complex interference environment.

The analysis of figures and tables clearly shows that the proposed PSSD algorithm has significantly improved demodulation performance under various conditions, especially in low SNR and complex interference environments. This fully confirms its robustness and

superiority in eLoran signal demodulation and strongly demonstrates its great potential value in practical applications.

5. Conclusions

The eLoran system, a crucial GNSS auxiliary, is substantially affected by various interferences that can undermine the precision of PNT services. This study proposes a novel PSSD algorithm to enhance the demodulation performance of eLoran signals in challenging noise and interference scenarios.

Key Contributions and Findings:

In summary, the implications of this study are twofold: enhancing the robustness and effectiveness of the current eLoran system and promoting the development and application of advanced signal processing techniques. The PSSD algorithm is a significant innovation in signal processing. Our findings show the positive impact of PSSD and lay a solid foundation for future signal processing research. The PSSD algorithm represents a significant innovation in signal processing.

1. Algorithm innovation: The PSSD algorithm utilizes advanced signal processing techniques in the frequency domain, including truncated window sampling and spectral smoothing, to effectively mitigate the impact of noise and interference, remarkably enhancing signal quality and demodulation accuracy.
2. Performance evaluation: Through well-designed experiments, we comprehensively evaluated the performance of the PSSD algorithm under diverse conditions. The experimental results indicate that the PSSD algorithm outperforms the traditional EPD algorithm in all tested situations, particularly in low SNR and complex interference environments

Limitations and Future Work:

Although the PSSD algorithm has shown excellent performance in theory and experiments, this study has certain limitations. For example, the constraints of receiving terminal hardware and available computational resources may pose challenges to the practical application of the algorithm. Future research needs to address these issues and further optimize the algorithm and explore new types of algorithms. The following specific directions are worthy of exploration:

1. Hardware implementation and testing: Implement the PSSD algorithm in actual eLoran receivers and test it under a broader and more complex real environment to verify its universality and effectiveness.
2. Algorithm optimization: Develop more efficient algorithm variants or optimization strategies to reduce computational complexity and enhance adaptability to limited-resource hardware.
3. Hardware upgrade and acceleration: Explore improving signal sampling rates and using dedicated accelerators like FPGA to improve the algorithm's performance and enable it to handle complex tasks more efficiently.
4. Algorithm expansion: Explore the application of classic digital signal processing algorithms such as DACM, SVD, and PSI in eLoran demodulation. Analyze their theoretical compatibility with eLoran signals; design implementations and conduct tests under various SNR and interference settings to identify their advantages and disadvantages, thus paving the way for potential integration with the PSSD algorithm.

In conclusion, the PSSD algorithm represents a significant step forward in the field of eLoran signal demodulation, offering an effective technical means to the challenges posed by noise and interference. Future research will continue to optimize the algorithm, explore its potential applications in broader scenarios, and ensure the continuous progress and innovation of eLoran systems in the field of communication for the benefit of reliable navigation.

Author Contributions: Conceptualization, S.L. and S.Z.; methodology, S.L.; software, S.L. and W.K.; validation, S.L. and B.Y.; formal analysis, S.L and L.X.; investigation, S.L.; resources, Y.H. and S.Z.; data curation, S.L.; writing—original draft preparation, S.L.; writing—review and editing, B.Y.; visualization, S.L. and W.K.; supervision, W.K.; project administration, Y.H.; funding acquisition, J.L. and L.X. All authors have read and agreed to the published version of the manuscript.

Funding: This work was mainly supported by the Natural Science Foundation of Sichuan Province (No. 2024NSFSC0841) and the Soft Science Project of China Meteorological Administration (No. 23ZDXM23).

Data Availability Statement: Data underlying the results presented in this paper are not completely publicly available at this time due to research project restrictions, but may be obtained from the authors upon reasonable request.

Acknowledgments: The authors would like to thank the institutions, teachers, and colleagues who provided the data collection site and platform for our work. We are also particularly grateful to the reviewers and editors for their insights and professional opinions that greatly assisted the research.

Conflicts of Interest: The authors declare no conflicts of interest.

References

1. Dardanelli, G.; Maltese, A. On the accuracy of cadastral marks: Statistical analyses to assess the congruence among GNSS-based positioning and official maps. *Remote Sens.* **2022**, *14*, 4086. [CrossRef]
2. Son, P.W.; Park, S.G.; Han, Y.; Seo, K.; Fang, T.H. Demonstration of the Feasibility of the Korean eLoran System as a Resilient PNT in a Testbed. *Remote Sens.* **2023**, *15*, 3586. [CrossRef]
3. Grant, A.; Williams, P.; Ward, N.; Basker, S. GPS Jamming and the Impact on Maritime Navigation. *J. Navig.* **2009**, *62*, 173–187. [CrossRef]
4. Dinesh, S. Globle Navigation Satellite System (GNSS) Spoofing: A Review of Growing Risks and Mitigation Steps. *Def. ST Tech. Bull.* **2013**, *6*, 42–61.
5. Hussain, A.; Akhtar, F.; Khand, Z.H.; Rajput, A.; Shaukat, Z. Complexity and Limitations of GNSS Signal Reception in Highly Obstructed Enviroments. *Eng. Technol. Appl. Sci. Res.* **2021**, *11*, 6864–6868. [CrossRef]
6. Zidan, J.; Adegoke, E.I.; Kampert, E.; Birrell, S.A.; Ford, C.R.; Higgins, M.D. GNSS Vulnerabilities and Existing Solutions: A Review of the Literature. *IEEE Access* **2021**, *9*, 153960–153976. [CrossRef]
7. Ward, N.; Hargreaves, C.; Williams, P.; Bransby, M. Delivering resilient PNT. In Proceedings of the 2015 International Association of Institutes of Navigation World Congress (IAIN), Prague, Czech Republic, 20–23 October 2015. [CrossRef]
8. Williams, P.; Basker, S.; Ward, N. e-Navigation and the Case for eLoran. *J. Navig.* **2008**, *61*, 473–484. [CrossRef]
9. Johnson, G.; Shalaev, R.; Hartnett, R.; Swaszek, P.; Narins, M. Can LORAN meet GPS backup requirements? *IEEE Aerosp. Electron. Syst. Mag.* **2005**, *20*, 3–12. [CrossRef]
10. Narkus-Kramer, M.; Scales, W.; Calle, E. Evaluating eLORAN as a backup for surveillance and navigation: A comparative cost analysis. In Proceedings of the 2009 IEEE/AIAA 28th Digital Avionics Systems Conference, Orlando, FL, USA, 23–29 October 2009. [CrossRef]
11. Johnson, G.W.; Swaszek, P.F.; Hartnett, R.J.; Shalaev, R.; Wiggins, M. An Evaluation of eLoran as a Backup to GPS. In Proceedings of the 2007 IEEE Conference on Technologies for Homeland Security, Woburn, MA, USA, 16–17 May 2007. [CrossRef]
12. Yan, W.H.; Zhao, K.J.; Li, S.F.; Wang, X.H.; Hua, Y. Precise Loran-C Signal Acquisition Based on Envelope Delay Correlation Method. *Sensors* **2020**, *20*, 2329. [CrossRef]
13. Liu, S.Y.; Zhang, S.G.; Hua, Y. A Cycle Identification Algorithm for enhanced LOng RAnge Navigation Signal Based on Skywave Reconstruction Technology. *J. Electron. Inf.* **2022**, *44*, 3592–3601. [CrossRef]
14. Li, S.F.; Wang, Y.L.; Hua, Y.; Xu, Y.L. Research of Loran-C data demodulation and decoding technology. *Chin. J. Sci. Instrum.* **2012**, *33*, 1407–1413. [CrossRef]
15. Lo, S.C.; Peterson, B.B.; Enge, P.K. Loran Data Modulation: A Primer[AESS Tutorial IV]. *IEEE Aerosp. Electron. Syst. Mag.* **2007**, *22*, 31–51. [CrossRef]
16. Yuan, J.B.; Yan, W.H.; Li, S.F.; Hua, Y. Demodulation Method for Loran-C at Low SNR Based on Envelope Correlation–Phase Detection. *Sensors* **2020**, *20*, 4535. [CrossRef] [PubMed]
17. Lyu, B.Y.; Hua, Y.; Yan, W.H.; Yuan, J.B.; Li, S.F. Data demodulation algorithm of enhanced Loran system. In Proceedings of the International Conference on Electronic Information Technology (EIT 2022), Chengdu, China, 18–20 March 2022. [CrossRef]
18. Liu, S.Y.; Yan, B.R.; Guo, W.; Hua, Y.; Zhang, S.G.; Lu, J.; Xu, L.; Yang, D. Research on ELoran Demodulation Algorithm Based on Multiclass Support Vector Machine. *Remote Sens.* **2024**, *16*, 3349. [CrossRef]
19. Kulmer, J.; Mowlaee, P. Phase Estimation in Single Channel Speech Enhancement Using Phase Decomposition. *IEEE Signal Process. Lett.* **2015**, *22*, 598–602. [CrossRef]
20. Liu, B.; Wang, Y.; Wang, W. Spectrogram enhancement algorithm: A soft thresholding-based approach. *Ultrasound Med. Biol.* **1999**, *25*, 839–846. [CrossRef]

21. Goryawala, M.; Sullivan, M.; Maudsley, A.A. Effects of apodization smoothing and denoising on spectral fitting. *Magn. Reson. Imaging* **2020**, *70*, 108–114. [CrossRef]
22. Huang, H.; Deng, L.; Zhou, L.; Dong, J. New Algorithm for Peak Alignment of Nuclear Magnetic Resonance. *Ele-Optic Technol. Appl.* **2013**, *28*, 51–54, 70.
23. Koziol, P.; Raczkowska, M.K.; Skibinska, J.; Urbaniak-Wasik, S.; Paluszkiewicz, C.; Kwiatek, W.; Wrobel, T.P. Comparison of spectral and spatial denoising techniques in the context of High Definition FT-IR imaging hyperspectral data. *Sci. Rep.* **2018**, *8*, 14351. [CrossRef] [PubMed]
24. Liang, J.; Zhang, L.; Luo, Z.; Jiang, R.; Cheng, Z.; Wang, S.; Sun, M.; Jun, S.; Cheng, Q.; Cui, T. A filtering reconfigurable intelligent surface for interference-free wireless communications. *Nat. Commun.* **2024**, *15*, 3838. [CrossRef]
25. Bayram, I. Employing phase information for audio denoising. In Proceedings of the 2014 IEEE International Conference on Acoustics, Speech and Signal Processing (ICASSP), Florence, BC, Italy, 4–9 May 2014. [CrossRef]
26. Masuyama, Y.; Yatabe, K.; Oikawa, Y. Low-rankness of Complex-valued Spectrogram and Its Application to Phase-aware Audio Processing. In Proceedings of the 2019 IEEE International Conference on Acoustics, Speech and Signal Processing (ICASSP), Brighton, UK, 12–17 May 2019. [CrossRef]
27. Helwig, A.; Offermans, G.; Stout, C.; Schue, C. eLoran System Definition and Signal Specification Tutorial. International Loran Association. 2011. Available online: http://www.ursanav.com/wp-content/uploads/UrsaNav-ILA-40-eLoran-Signal-Specification-Tutorial.pdf (accessed on 30 October 2024).
28. Van Willigen, D.; Offermans, G.W.A.; Helwig, A.W.S. EUROFIX: Definition and current status. In Proceedings of the IEEE 1998 Position Location and Navigation Symposium, Palm Springs, CA, USA, 20–23 April 1998. [CrossRef]
29. Offermans, G.W.A.; Helwig, A.W.S.; van Willigen, D.V. Eurofix System and its Developments. *J. Navig.* **1999**, *52*, 163–175. [CrossRef]
30. Williams, P.; Last, D. Modelling Loran-C envelope-to-cycle differences in mountainous terrain. In Proceedings of the 32nd Annual Meeting, International Loran Association, Boulder, CO, USA, 3–6 November 2023.
31. *GB/T 12752-1991*; General Specification for Marine Loran-C Receiving Equipment. The State Bureau of Quality and Technical Supervision: Beijing, China, 1991. Available online: https://www.renrendoc.com/p-881056.html (accessed on 5 December 2024).
32. Safar, J.; Williams, P.; Grant, A.; Vejrazka, F. Analysis, modelling and mitigation of cross-rate interference in eLoran. *J. Navig.* **2016**, *63*, 295–319. [CrossRef]
33. Liu, S.Y.; Zhang, S.G.; Hua, Y. Research on GRI Combination Design of eLORAN System. *J. Electron. Inf.* **2022**, *44*, 767–774. [CrossRef]
34. Yan, W.H.; Dong, M.; Li, S.F.; Yang, C.Z.; Yuan, J.B.; Hu, Z.P.; Hua, Y. An eLoran Signal Cycle Identification Method Based on Joint Time–Frequency Domain. *Remote Sens.* **2022**, *14*, 250. [CrossRef]
35. Liu, S.Y. Study on Interference Processing Methods and Techniques of eLoran System. Ph.D. Thesis, University of Chinese Academy of Sciences (National Time Service Center), Xi'an, China, 2022.
36. *SAE 9990/1-2018*; Transmitted Enhanced Loran (eLoran) Signal Standard for Tri-State Pulse Position Modulation. SAE International: Warrendale, PA, USA, 2018.
37. Wu, H.T.; Li, X.H.; Zhang, H.J.; Gao, H.J.; Bian, Y.J. UTC message broadcasting over Loran-C data channel. In Proceedings of the 2002 IEEE International Frequency Control Symposium and PDA Exhibition (Cat. No.02CH37234), New Orleans, LA, USA, 31 May 2002. [CrossRef]
38. Lo, S.C.; Peterson, B.B.; Enge, P.K.; Swaszek, P. Loran data modulation: Extensions and examples. *IEEE Trans. Aerosp. Electron. Syst.* **2007**, *43*, 628–644. [CrossRef]
39. Wu, B.; Li, Y.; Zhang, D.L. Based on reed solomon code design of a flash memory controller. *Electr. Measur. Technol.* **2011**, *34*, 12–17.
40. Wang, H.S.; Ma, C.; Jia, H.B. Application of low complexity Reed-Solomon decoder in seismic exploration. *Chin. J. Sci. Instrum.* **2010**, *31*, 1632–1637.
41. Sooch, S.K.; Gupta, M.; Kumar, R. Implementing Cyclic Redundancy Check as Error Correction Technique in HDLC. *Ann. Com. Sci. Inf. Sys.* **2020**, *24*, 131–136. [CrossRef]
42. Ahmad, M.; Rahman, S. Design of HDLC Controller with CRC Generation Using VHD. *IJMER* **2014**, *4*, 8–12.
43. Li, S.F. Study on The Methods and Techniques of ELoran Signal Received. Ph.D. Thesis, University of Chinese Academy of Sciences (National Time Service Center), Xi'an, China, 2013.